Ab Initio Study of the Structural, Electronic, Magnetic, and Hyperfine Properties of GaxFe4−xN (0.00 ≤ x ≤ 1.00) Nitrides

ARTICLE *in* THE JOURNAL OF PHYSICAL CHEMISTRY C · NOVEMBER 2011

Impact Factor: 4.77 · DOI: 10.1021/jp205060h

6 AUTHORS, INCLUDING:

Arles Gil Rebaza
Institute of Physic La Plata
13 PUBLICATIONS **31** CITATIONS
SEE PROFILE

Sajith Kurian
Hanyang University
24 PUBLICATIONS **138** CITATIONS
SEE PROFILE

Sayan Bhattacharyya
Indian Institute of Science Education and Re…
61 PUBLICATIONS **647** CITATIONS
SEE PROFILE

Eitel Peltzer
National University of La Plata
56 PUBLICATIONS **642** CITATIONS
SEE PROFILE

THE JOURNAL OF PHYSICAL CHEMISTRY C

ARTICLE

pubs.acs.org/JPCC

Ab Initio Study of the Structural, Electronic, Magnetic, and Hyperfine Properties of $Ga_xFe_{4-x}N$ ($0.00 \leq x \leq 1.00$) Nitrides

Arles V. Gil Rebaza,[†] Judith Desimoni,[†] Sajith Kurian,[§] Sayan Bhattacharyya,[∥] Namdeo S. Gajbhiye,[§,∥] and Eitel L. Peltzer y Blancá[*,‡]

[†]Departamento de Física, Facultad de Ciencias Exactas - UNLP, IFLP-CONICET, CC 67, 1900 La Plata, Argentina

[‡]Grupo de Estudio de Materiales y Dispositivos Electrónicos (GEMyDE), Facultad de Ingeniería - UNLP, IFLYSIB-CONICET, CC No. 565, 1900 La Plata, Argentina

[§]Department of Chemistry, Indian Institute of Technology, Kanpur 208016, U.P., India

[∥]Department of Chemical Sciences, Indian Institute of Science Education and Research, Kolkata, Mohanpur 741252, Nadia, W.B., India

ABSTRACT: The dependence with Ga content (x) of structural, magnetic, and hyperfine properties of $Ga_xFe_{4-x}N$ compounds has been studied using the full-potential linearized augmented planewave method based on density functional theory. A nonlinear increase of the lattice parameter with x was observed, ascribed to the different metallic radii of Fe and Ga atoms and a magneto-volumetric effect. The magnetic moment per formula unit (M_{fu}) decreases linearly with x, where the M_{fu} of $GaFe_3N$ is almost half for the corresponding value of γ'-Fe_4N, mainly due to the decreasing of magnetic moment of the FeII (3c Wyckoff position) atoms with the number of Ga next nearest neighbors (nnn). The hyperfine parameters of the FeI (1a Wyckoff position) do not change with x, whereas the hyperfine field (B_{hf}), isomer shift (δ), and quadrupole shift (ε) of the FeII atoms depend linearly with nnn Ga atoms. Furthermore, by use of fixed spin moment calculation to obtain the curve M_{fu} vs total energy, it was possible to determine that the ground state of $GaFe_3N$ belongs to a ferrimagnetic configuration with a lattice parameter similar to the experimental value.

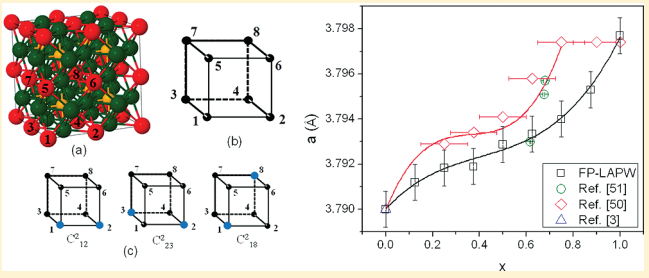

1. INTRODUCTION

The potential technological applications as high-density magnetic recording have propelled the 3d transition metal nitrides to be one of the most researched materials.[1−4] Metal nitrides also exhibit significantly high electrical resistivity and wear resistance[5] and have been the subject of experimental and theoretical studies from chemical, thermal, mechanical, electrical, magnetic, and microstructural points of view.[4−11] Among the nitrides, γ'-Fe_4N has been investigated theoretically[8−10,12−18] and experimentally[3−5,11,19−22] since it is a promising candidate for high density recording material due to its large saturation magnetization and good chemical stability. The γ'-Fe_4N has an antiperovskite type structure (space group Pm-$3m$)[23] where the Fe atoms occupy the corners (FeI) and the center of the faces (FeII), while the N atoms are placed at the center of the cube.

To improve the magnetic properties of γ'-Fe_4N, the isomorphic compound MFe_3N (where M is a metal, M = Ni,[24−32] Pt,[8,25,33,34] Pd,[25,35−37] Co,[38−41] Rh,[7,8,39,42] Ir,[6,8,39] Ru,[6,10,43,44] Os,[6,9,43,44] etc.) has been studied. These compounds are isostructural to γ'-Fe_4N, in which Fe−N layers are interlayered with Fe−M layers and M atoms can substitute either FeI or FeII atoms. It is known that metal atoms can replace Fe ones at the corner of the cube if their chemical affinity for nitrogen atoms is weaker than iron−nitrogen affinity. On the other hand, some M atoms can occupy crystallographic nonequivalent iron sites, without any particular site preference.[45−47] However, in the case of atoms with metallic radius larger than that of the Fe atom, the position FeI is preferred as the coordination sphere of this site is much larger than the FeII one. This is the case of gallium since its metallic radius (1.41 Å[48]) is larger than that of iron (1.26 Å[48]). Few theoretical and experimental reports on the $Ga_xFe_{4-x}N$ system have been published.[49−52]

Herein our study is based on the ab initio calculations of equilibrium lattice constant, magnetic moments, and hyperfine parameters of $Ga_xFe_{4-x}N$ to ascertain the compositional and functional properties of the compound, by changing the concentration of Ga content between x = 0.00 to 1.00. To find the equilibrium configurations and the above-mentioned properties, different Fe−Ga−N configurations that gave rise to supercells were considered. The calculations were performed using the full-potential linearized augmented plane-wave (FP-LAPW) method within the framework of density functional theory (DFT)[53−56] as implemented in the Wien2K code.[57] The results are compared with experimental values and discussed.

Received: May 30, 2011
Revised: September 27, 2011
Published: October 03, 2011

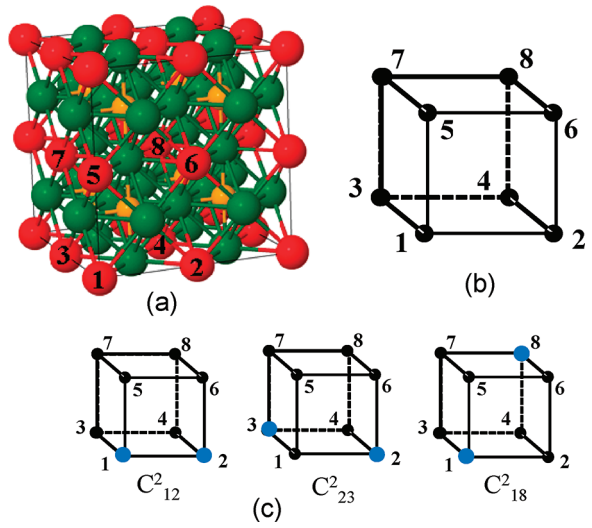

Figure 1. (a) 2 × 2 × 2 supercell of γ'-Fe_4N consisting of FeI (red), FeII (green), and N (orange) atoms. (b) Cubic sublattice formed by FeI atoms (sites 1, 2, 3, 4, 5, 6, 7, and 8). (c) Nonequivalent configurations, C^2_{12}, C^2_{23}, and C^2_{18}, arising from the replacement of two FeI atoms by Ga (blue) to obtain the value of x = 0.250 (see Table 1).

2. COMPUTATIONAL DETAILS

The calculations were performed using FP-LAPW method within the framework of DFT[53−56] as implemented in the Wien2K code.[57] In this scheme, the exchange-correlation potential for structural, electronic, magnetic, and hyperfine properties were calculated using generalized gradient approximation (GGA) based on the Perdew−Burke−Ernzerhof expression.[56,58] The parameter $R_{MT} \times K_{max}$ was kept equal to 9 (R_{MT} is the muffin-tin radius and K_{max} the largest K vector in the plane wave expansion). The Muffin-tin radii employed for Ga ($4s^2 3d^{10} 4p^1$), Fe ($4s^2 3d^6$), and N ($2s^2 2p^3$) were 2.59, 1.79, and 1.59 bohr, respectively. A mesh of 286 k-points was taken in the irreducible edge of the Brillouin Zone. The total energy was converged to 10^{-6} Ry. In all calculations, the core and valence states are treated in the fully and scalar relativistic scheme, respectively; spin polarization was considered, in addition to the nonmagnetic and magnetically ordered configurations.

3. METHODOLOGY

The γ'-Fe_4N has an antiperovskite cubic structure, *Pm*-3*m* space group, where two types of Fe atoms can be distinguished, FeI and FeII, located in the corner of the cube and in the center of the face (1a and 3c, according to Wyckoff notation), respectively, while N atoms occupy the center of the cube (1b Wyckoff site).[3,23] In the present work to obtain the different Ga concentrations (x), a 2 × 2 × 2 supercell of γ'-Fe_4N was employed. This supercell has 40 atoms, divided in the following classes: 8 FeI atoms (sites 1, 2, 3, 4, 5, 6, 7, and 8, Figure 1a) forming a cubic sublattice (Figure.1b), 24 FeII atoms, and 8 N atoms. The Ga atoms substitute FeI in the supercell, as was suggested in experimental work,[50] and will be named GaI hereafter. The ratio GaI:FeI and the total number of Fe sites give the x content value in the ternary $Ga_xFe_{4-x}N$. It is worth mentioning that nonequivalent atomic configurations are obtained for the same x value depending on the iron substituted site as shown in Figure 1b and quoted in Table 1. This configurations are denoted by $C^i_{j...k}$, where the superscript and subscript indicates the amount of FeI atoms replaced by Ga ones and the places in the cubic sublattice, respectively. For example, x = 0.250 contains 3 nonequivalent configurations, which are denoted by C^2_{12}, C^2_{23}, and C^2_{18}, observed in Figure 1c.

Table 1. GaI:FeI Ratios with the Corresponding x Content and the Different Configurations in the 2 × 2 × 2 Supercell

GaI:FeI	x	formula	configurations
0:8	0.000	γ'-Fe_4N	
1:8	0.125	$Ga_{0.125}Fe_{3.875}N$	C^1_1
2:8	0.250	$Ga_{0.250}Fe_{3.750}N$	C^2_{12}, C^2_{23}, C^2_{18}
3:8	0.375	$Ga_{0.375}Fe_{3.625}N$	C^3_{123}, C^3_{267}, C^3_{258}
4:8	0.500	$Ga_{0.500}Fe_{3.500}N$	C^4_{1234}, C^4_{1347}, C^4_{1345}, C^4_{1346}, C^4_{1368}, C^4_{1467}
5:8	0.625	$Ga_{0.625}Fe_{3.375}N$	C^5_{12345}, C^5_{13458}, C^5_{13467}
6:8	0.750	$Ga_{0.750}Fe_{3.250}N$	C^6_{123456}, C^6_{123458}, C^6_{123678}
7:8	0.875	$Ga_{0.875}Fe_{3.125}N$	$C^7_{2345678}$
8:8	1.000	$Ga_{1.000}Fe_{3.000}N$	$C^8_{12345678}$

For concentrations with more than one configuration, we choose the configuration of minimum energy; this criteria is described below. In the configuration chosen for each concentration, the atoms of Ga and Fe have different GaI, FeI, and FeII nearest neighbor (nn) and next near neighbor (nnn) arrangements, presented in Table 2. It is important to remark that the nomenclature used for each x value indicates the distinct neighborhood of the diverse kind of atoms in the ternary $Ga_xFe_{4-x}N$ compound, i.e., the FeI*i*, FeII*j*, and GaI*k* atoms have different local nn and nnn configurations depending on the Ga content.

4. RESULTS AND DISCUSSION

4.1. Structural Properties. For the different x values, the equilibrium lattice, magnetic, and hyperfine parameters were determined considering the energy of magnetic and nonmagnetic configurations. In all cases, the equilibrium configuration corresponds to a ferrimagnetic state with antiparallel interactions between Fe (FeI and FeII) and Ga atoms, where the atomic positions have been fixed. The different Ga−Fe atomic configurations displays different energy curves, as observed in Figure 2. The energy−lattice parameter curves were analyzed using third order Birch−Murgnahańs state equation.[59,60] The fitted values are quoted in Table 3.

The lattice parameters of the $Ga_xFe_{4-x}N$ (x = 0.000, 0.125, 0.250, 0.375, 0.500, 0.625, 0.750, and 1.000) have been experimentally determined twice from the same set of samples, using Cu and Mo Kα_1 radiations, showing contradictory results.[50,52] The refined lattice parameters obtained using the Cu Kα_1 radiation (λ = 1.54059 Å) indicated a good agreement with previous data for x = 0.00 and an increment of a with x to achieve a saturation value for x values higher than x = 0.750. The reported new lattice parameter values obtained using the Mo Kα_1 radiation (λ = 0.70932 Å) show a different behavior with x, ascribed to the differences between the covalent radii of Fe and Ga atoms. Moreover, the lattice parameter obtained for γ'-Fe_4N is quite high when compared with the previous reports.[3,50] Hence we will only consider the first set of data[50] in the present analysis, together with those obtained from ammonolysis reported in reference 51 using Cu Kα_1 radiation.

Table 2. Fe and Ga Local Configurations[a]

			x = 0.000			
			FeII*a* (8)			FeII*a* (24)
nn			12FeII*a*			2N
nnn			8N			4Fe*Ia*
						8FeII*a*
			x = 0.125			
	GaI*a* (1)	FeI*a* (3)	FeI*b* (3)	FeI*c* (1)	FeII*a* (12)	FeII*b* (12)
nn	12FeII*a*	8FeII*a*	4FeII*a*	12FeII*b*	2N	2N
		4FeII*b*	8FeII*b*			
nnn	8N	8N	8N	8N	1GaI*a*	1Fe*Ia*
					2Fe*Ia*	2Fe*Ib*
					1Fe*Ic*	1Fe*Ic*
					4FeII*a*	4FeII*a*
					4FeII*b*	4FeII*b*
			x = 0.250			
		GaI*a* (2)		FeI*a* (6)		FeII*a* (24)
nn		12FeII*a*		12FeII*a*		2N
nnn		8N		8N		1GaI*a*
						3Fe*Ia*
						8FeII*a*
			x = 0.375			
	GaI*a* (3)	FeI*a* (3)	FeI*b* (1)	FeI*c* (1)	FeII*a* (12)	FeII*b* (12)
nn	4FeII*a*	8FeII*a*	12FeII*a*	12FeII*b*	2N	2N
	8FeII*b*	4FeII*b*				
nnn	8N	8N	8N	8N	1GaI*a*	2GaI*a*
					2Fe*Ia*	1Fe*Ia*
					1Fe*Ib*	1Fe*Ic*
					4FeII*a*	4FeII*a*
					4FeII*b*	4FeII*b*
			x = 0.500			
	GaI*a* (3)	GaI*b* (1)	FeI*a* (3)	FeI*b* (1)	FeII*a* (12)	FeII*b* (12)
nn	8FeII*a*	12FeII*a*	4FeII*a*	12FeII*b*	2N	2N
	4FeII*b*		8FeII*b*			
nnn	8N	8N	8N	8N	2GaI*a*	1GaI*a*
					1GaI*b*	2Fe*Ia*
					1Fe*Ia*	1Fe*Ib*
					4FeII*a*	4FeII*a*
					4FeII*b*	4FeII*b*
			x = 0.625						
	GaI*a* (1)	GaI*b* (2)	GaI*c* (1)	GaI*d* (1)	FeI*a* (2)	FeI*b* (1)	FeII*a* (8)	FeII*b* (4)	FeII*c* (8)	FeII*d* (4)
nn	8FeII*a*	4FeII*a*	4FeII*b*	8FeII*a*	4FeII*a*	8FeII*c*	2N	2N	2N	2N
	4FeII*b*	4FeII*b*	8FeII*c*	4FeII*d*	4FeII*c*	4FeII*d*				
		4FeII*c*			4FeII*d*					
nnn	8N	8N	8N	8N	8N	8N	1GaI*a*	1GaI*a*	1GaI*b*	1GaI*d*
							1GaI*b*	2GaI*b*	1GaI*c*	2Fe*Ia*
							1GaI*d*	1GaI*c*	1Fe*Ia*	1Fe*Ib*

dx.doi.org/10.1021/jp205060h |*J. Phys. Chem. C* 2011, 115, 23081–23089

Table 2. Continued

				x = 0.625					
	GaIa (1)	GaIb (2)	GaIc (1)	GaId (1)	FeIa (2)	FeIb (1)	FeIIa (8)	FeIIb (4)	FeIIc (8)	FeIId (4)
							1FeIa	4FeIIa	1FeIb	4FeIIa
							2FeIIa	4FeIIc	2FeIIa	4FeIIc
							2FeIIb		2FeIIb	
							2FeIIc		2FeIIc	
							2FeIId		2FeIId	
				x = 0.750					
	GaIa (2)		GaIb (4)		FeIa (2)		FeIIa (8)	FeIIb (8)		FeIIc (8)
nn	4FeIIa		4FeIIa		4FeIIa		2N	2N		2N
	8FeIIb		4FeIIb		8FeIIc					
			4FeIIc							
nnn	8N		8N		8N		1GaIa	2GaIa		2GaIb
							2GaIb	2GaIb		2FeIa
							1FeIa	4FeIIa		4FeIIa
							4FeIIb	4FeIIb		2FeIIb
							4FeIIc	4FeIIc		2FeIIc
				x = 0.875					
	GaIa (3)		GaIb (3)		GaIc (1)		FeIa (1)	FeIIa (12)		FeIIb (12)
nn	8FeIIa		4FeIIa		12FeIIb		12FeIIb	2N		2N
	4FeIIb		8FeIIb							
nnn	8N		8N		8N		8N	2GaIa		1GaIa
								1GaIb		2GaIb
								1FeIa		1GaIc
								4FeIIa		4FeIIa
								4FeIIb		4FeIIb
				x = 1.000					
				GaIa (8)						FeIIa (24)
nn				12FeIIa						2N
nnn				8N						4GaIa
										8FeIIa

[a] The Ga and Fe nn and nnn atoms are indicated. The number between parentheses indicates the population of each kind of atoms in the supercell.

A comparison between the present calculated values and the reported experimental ones[3,50,51] are presented in Figure 3. The experimental and theoretical values follow the same trend, i.e., a nonlinear increment with x, probably related to the difference in the metallic radii between Fe and Ga atoms (r_{Fe} = 1.24 Å and r_{Ga} = 1.41 Å, respectively[48]) and a magneto-volumetric effect due to iron atoms. To calculate an error bar of the equilibrium lattice parameters, it was allowed a relaxation of the atomic positions to calculate a new lattice parameter vs energy curve, and so it was obtained the lattice parameter with relaxed atomic positions. The error bars indicate this variation of the lattice parameter in Figure 3. This process has been performed for x = 0.125 and 0.875, showing a minimal variation of the lattice parameter. Besides, these error bars have been considered for the remaining data (Figure 3).

The agreement between the calculated and experimental results is excellent for the extreme concentrations, x = 0.0000 and 1.000, while a negligible shift is observed for the intermediate Ga concentrations.

Since the system is not a random solid solution, both experimental and calculated data were fitted by considering a third order polynomial.[61] The resulting polynomials are

$$a^{cal}(x) = 3.7900_2(1-x) + 3.7976_2x + 0.0040_2x(1-x)^2 - 0.0130_2x^2(1-x) \quad (1)$$

$$a^{exp}(x) = 3.7899_2(1-x) + 3.8050_2x + 0.0060_7x(1-x)^2 - 0.0600_2x^2(1-x) \quad (2)$$

Again, a good agreement between experimental and calculated polynomial parameters, when considering the fitting errors, can be observed. The slight discrepancies could be ascribed to the fact that calculations are performed assuming 0 K, while the experimental data were recorded at room temperature.

4.2. Electronic Structure and Magnetic Properties. The electronic density of states (DOS) for the different atomic species of $Ga_xFe_{4-x}N$ is show in Figure 4, for $x = 0.00$, 0.50, and 1.00. The Fe^I states are concentrated between the E_F and −5.0 eV, while the DOS corresponding to FeII spread up to −7.0 eV for γ'-Fe_4N and expanding to −9.0 eV for $GaFe_3N$ (parts a and b of Figure 4). The N states lie between −4.0 and −7.0 eV for γ'-Fe_4N and spread to lower energies when the FeI atoms are replaced by Ga ones (parts a−c of Figure 4), whereas the Ga states are located between −5.0 and −9.0 eV and the population of some electronic states close to −4.0 eV for the $GaFe_3N$ (Figure 4c).

The projected DOS for $x = 0.50$ and 1.00 is shown in Figure 5, where it is possible see a noticeable hybridization between s-GaI, p-N, and d-FeII orbitals concentrated between −5.0 and −9.0 eV (parts b and c of Figure 5), pointing toward a direct interaction among FeII and nnn GaI atoms. Also, a weak hybridization is observed linking the d-FeII and p-Ga orbitals located between −2.0 to −5.0 eV, more notable for $x = 1.00$ (parts b and c of Figure 5).

Moreover, as the x content increases a shift of the up-FeII DOS to energies higher than the E_F is detected, while the down-DOS moves in the opposite direction, as observed in the trend of the d-FeII charges. While the up-FeII charge increases with x, the opposite is observed for the down-FeII charge (Figure 6),

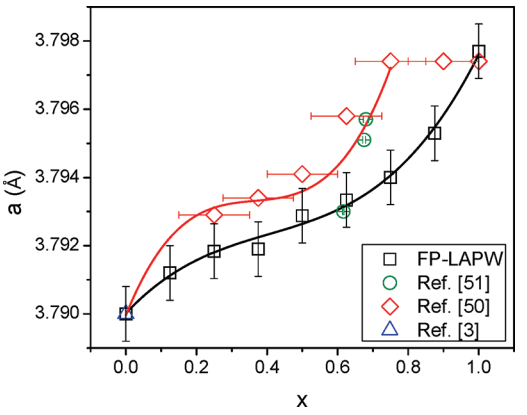

Figure 3. Evolution with Ga content (x) of the experimental[3,50,51] and calculated lattice parameter values. Solid lines correspond to the fitting using a third-order polynomial, eqs 1 and 2.

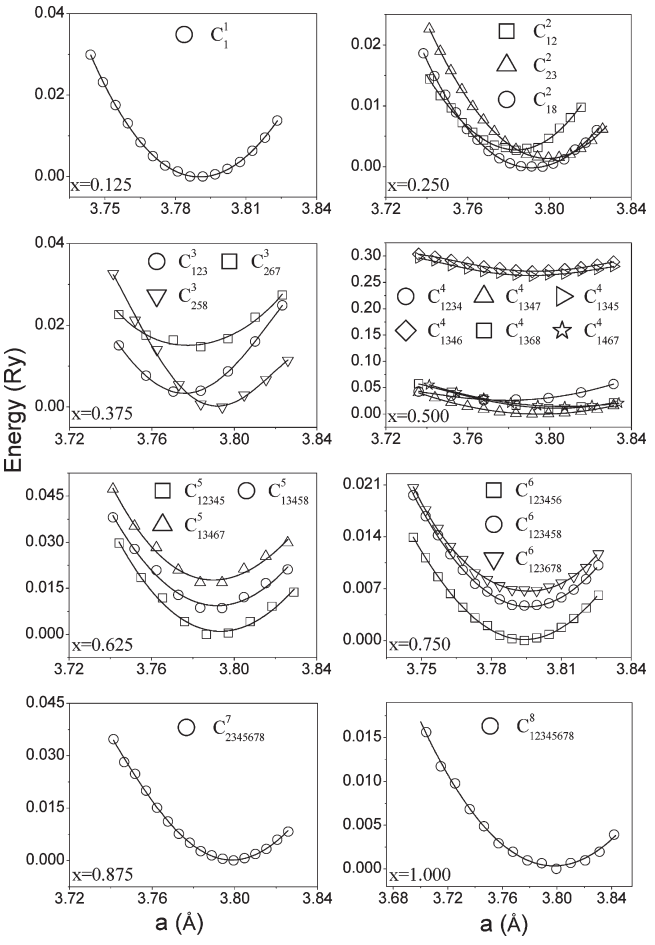

Figure 2. Energy vs lattice parameter curves for the different configurations labeled with the Ga content in $Ga_xFe_{4-x}N$.

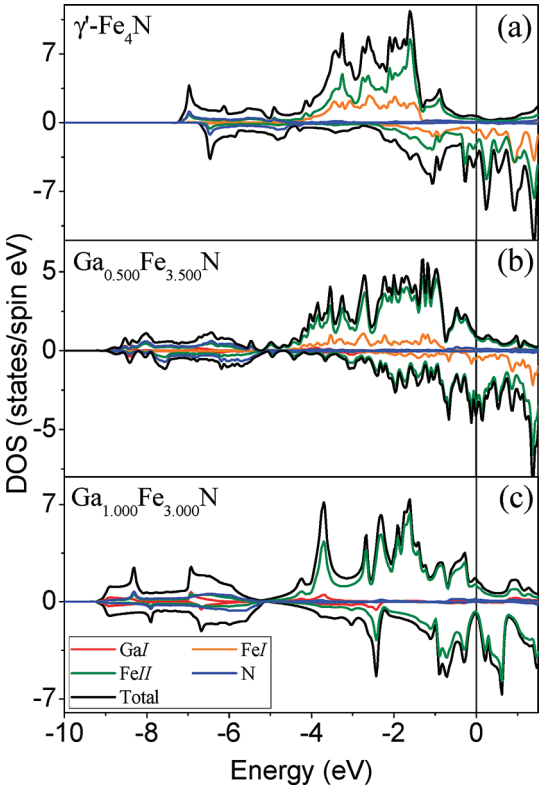

Figure 4. Total DOS with the different atomic contribution for (a) γ'-Fe_4N, (b) $Ga_{0.50}Fe_{3.50}N$, and (c) $Ga_{1.00}Fe_{3.00}N$.

Table 3. Equilibrium Lattice Parameters (a) and Bulk Modulus (B) of the $Ga_xFe_{4-x}N$

x	0.000	0.125	0.250	0.375	0.500	0.625	0.750	0.875	1.000
configuration		$C^1{}_1$	$C^2{}_{18}$	$C^3{}_{258}$	$C^4{}_{1347}$	$C^5{}_{12345}$	$C^6{}_{123456}$	$C^7{}_{2345678}$	$C^8{}_{12345678}$
a (Å)	3.7900	3.7912	3.7918	3.7919	3.7929	3.7933	3.7940	3.7953	3.7977
B (GPa)	200	206	205	204	197	180	167	177	217

dx.doi.org/10.1021/jp205060h |J. Phys. Chem. C 2011, 115, 23081–23089

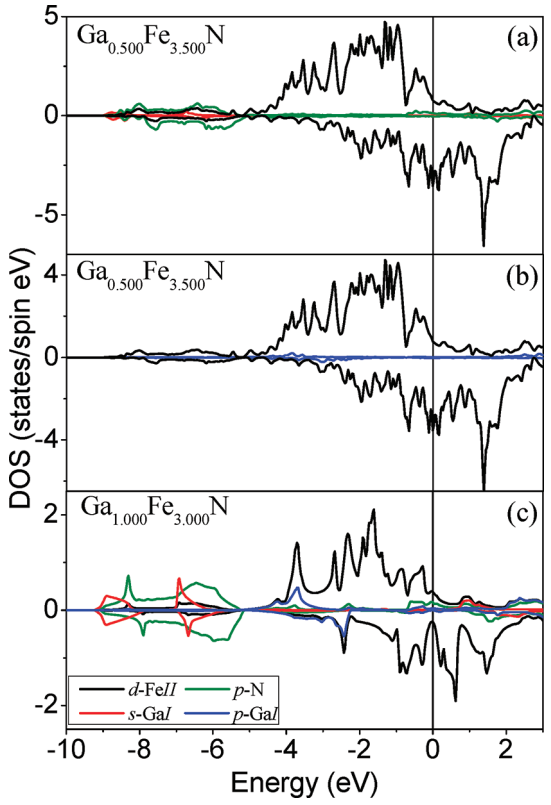

Figure 5. Projected DOS showing the hybridization between the orbitals (a) s-GaI, d-FeII, and p-N, (b) p-GaI and d-FeII for $Ga_{0.50}Fe_{3.50}N$, and (c) idem to parts a and b for $Ga_{1.00}Fe_{3.00}N$.

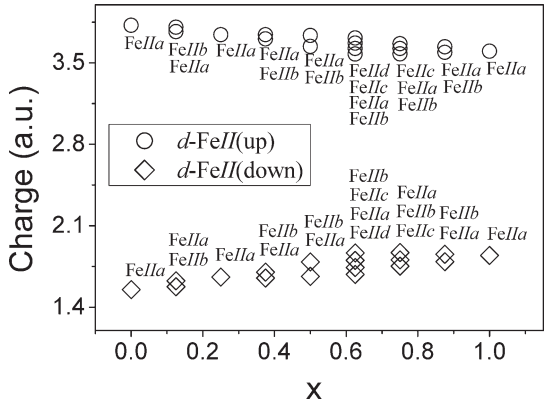

Figure 6. Total charge of the d-FeII orbitals in function of the *x*. The nomenclature for the FeII sites corresponds to the one used in Table 2.

involving a decrease of the magnetic moment of the FeII atoms with *x*. The evolution of the DOS of the FeII and GaI atoms gives rise to a decrease of the magnetic moment per formula unit (M_{fu}), as seen in Figure 7a. In effect, a linear decreasing trend of the magnetic moment per formula unit with *x* is established, $dM_{fu}/dx = -4.6\ \mu_B$/Ga atom, and the resulting M_{fu} of $GaFe_3N$ is half to that of γ'-Fe_4N. The calculated and experimental ($dM_{fu}/dx = -9.7\ \mu_B$/Ga atom) values of the magnetic moment per formula unit have different slopes. The experimentally determined magnetic moment per formula unit for $GaFe_3N$ was 0.87 μ_B,[51,52] much smaller than the calculated one (5.3 μ_B).

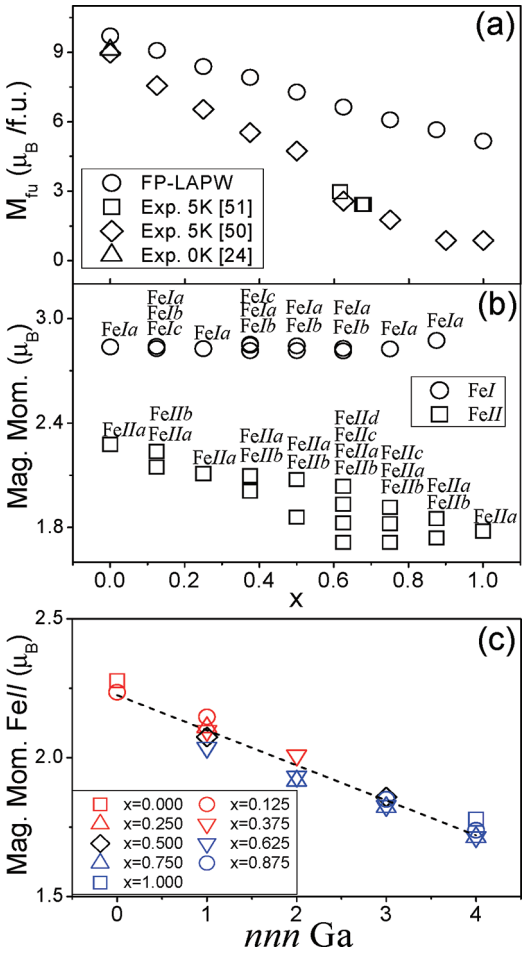

Figure 7. Evolution of the magnetic moment with Ga content of (a) formula unit (ref 24: extrapolate to 0 K), (b) FeII and FeI atoms (the nomenclature for the FeI and FeII sites corresponds to the one used in Table 3), and (c) FeII magnetic moment vs the number of next nearest Ga neighbors.

The FeI magnetic moment remains nearly constant for the different concentrations of Ga, while the FeII one decreases linearly with the increment of the Ga concentration (Figure 7b), with a slope of $-0.13\ \mu_B$ per nnn Ga atom (Figure 7c), probably related with the chemical bonding between them. Ga atoms show a small magnetic moment ($-0.11\ \mu_B$), which interacts weakly with Fe atoms through an antiferromagnetic coupling.

4.3. Structural and Magnetic Stability of $GaFe_3N$. According to the experimental findings, $GaFe_3N$ is ferrimagnetic and has a magnetic moment of 0.87 μ_B per formula unit,[50,52] while the same authors report a calculation of the magnetic moment of 5 μ_B per formula unit,[52] similar to the obtained in the present article (5.3 μ_B per formula unit).

To study the stability of $GaFe_3N$, the total energy vs lattice parameter curves were obtained for the nonmagnetic and ferrimagnetic states. It is observed in Figure 8 that the ground state is ferrimagnetic. To get a deeper knowledge about ground state of this material, we have performed fixed spin moment calculations to obtain the equilibrium lattice parameter for different values of magnetic moment per formula unit from 0.5 to 6 μ_B. In Figure 9a, the variation of the equilibrium lattice parameter with the magnetic moment per formula unit is presented. The lattice parameters obtained are 3.7270 Å for

dx.doi.org/10.1021/jp205060h |J. Phys. Chem. C 2011, 115, 23081–23089

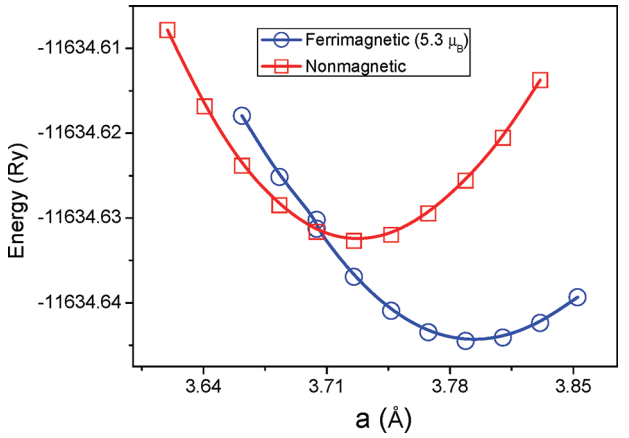

Figure 8. $GaFe_3N$ energy vs lattice parameter curves.

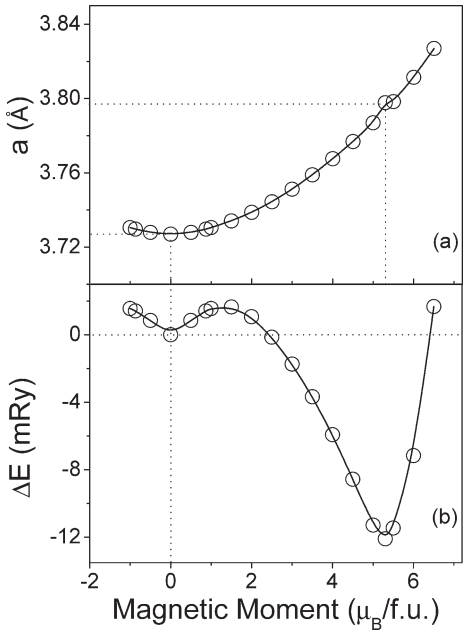

Figure 9. (a) Variation of the equilibrium lattice parameter as function of the magnetic moment per formula unit of $GaFe_3N$. (b) The variation of the energy as a function of the magnetic moment per formula unit.

the nonmagnetic state and 3.7977 Å for the ferrimagnetic state with 5.3 μ_B per formula unit.

Figure 9b shows the variation of the energy vs magnetic moment per formula unit, with respect to the nonmagnetic state. The minimum of curve belongs to the ferrimagnetic state, while a local minimum represent the nonmagnetic state. Furthermore, from Figure 9b an energy barrier is observed between nonmagnetic and ferrimagnetic states, with a height of 1.6 mRy, whereas from the ferrimagnetic to nonmagnetic states the barrier height is 12 mRy.

4.4. Hyperfine Properties. Going further with the characterization of the $Ga_xFe_{4-x}N$, the magnetic hyperfine field (B_{hf}), the isomer shift (δ) referred to α-Fe, and the quadrupole shift (ε) were calculated. The B_{hf} was calculated using only the contact term since it is the major contribution.[62−64] To evaluate δ and ε, $\alpha = -0.22\ a_0^{-2}$ mm/s[65] and $Q_N = -0.16$ b[66] were used, respectively.

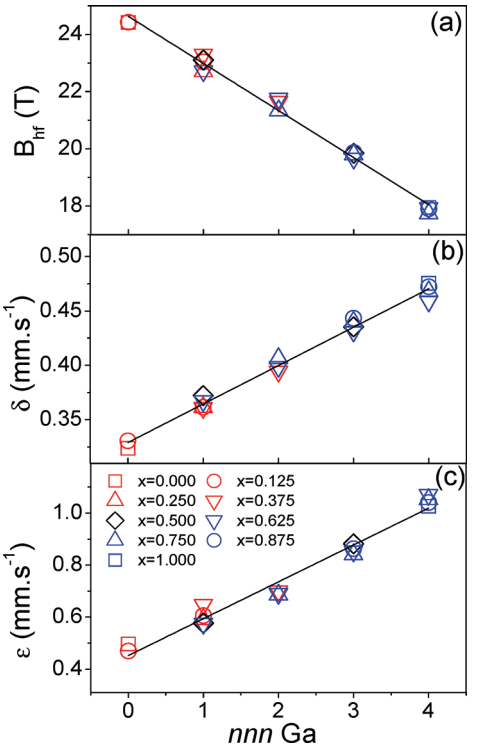

Figure 10. Dependence of the hyperfine parameters of FeII with the number of nnn Ga atoms. (a) Hyperfine field (B_{hf}), (b) isomer shift (δ), and (c) quadrupole shift (ε).

The hyperfine field of FeI site ranges between 36.9 and 41.3 T. It is also observed that the FeI isomer and quadrupole shifts remain nearly constant with x, ranging between 0.28 and 0.30 mm/s and 0.00 and 0.09 mm/s, respectively. Whereas B_{hf} of the FeII site gradually decreases with concentration of Ga. This kind of variation of the hyperfine field with Ga concentration has been reported in Fe−Ga alloys.[67,68] Associated with a decrease of the density of charge, mainly the s-FeII orbitals, the isomer shift values corresponding to FeII increase with Ga content. The same behavior was detected in Fe−Ga solid solutions.[68,69] A similar trends with the Ga content is observed for the quadrupole shift of FeII showing a major cubic asymmetry of the $Ga_xFe_{4-x}N$. A closer analysis of the calculated parameters reveals that the hyperfine parameters associated to the FeII site mainly depends on the number of nnn Ga atoms, as observed in Figure 10a. In effect, the presence of a nnn Ga atom reduces the hyperfine field in −1.65 T/Ga atom and increases the isomer and the quadrupole shifts by 0.04 and 0.14 mm s^{-1}/Ga atom, respectively (parts b and c of Figure 10).

To help in the analysis and interpretation of the $Ga_xFe_{4-x}N$ Mössbauer spectra[51] the hyperfine field distributions have been calculated (Figure 11). The distributions are complex and present several maxima depending on the Ga content. In effect, the Mössbauer spectra recorded at 5 K from samples prepared using a controlled one-step ammonolysis method[51] show a complex structure that was reproduced with a distribution of the hyperfine field with several wide maxima as a consequence of Ga concentration gradient. However, from the theoretical distributions, presented in Figure 11, assuming ordered phases, it can be concluded that the average hyperfine field decreases with Ga content, from 24 to 18 T. The present calculations should indicate, considering the Mössbauer spectral resolution, (2 T[64]),

dx.doi.org/10.1021/jp205060h |J. Phys. Chem. C 2011, 115, 23081–23089

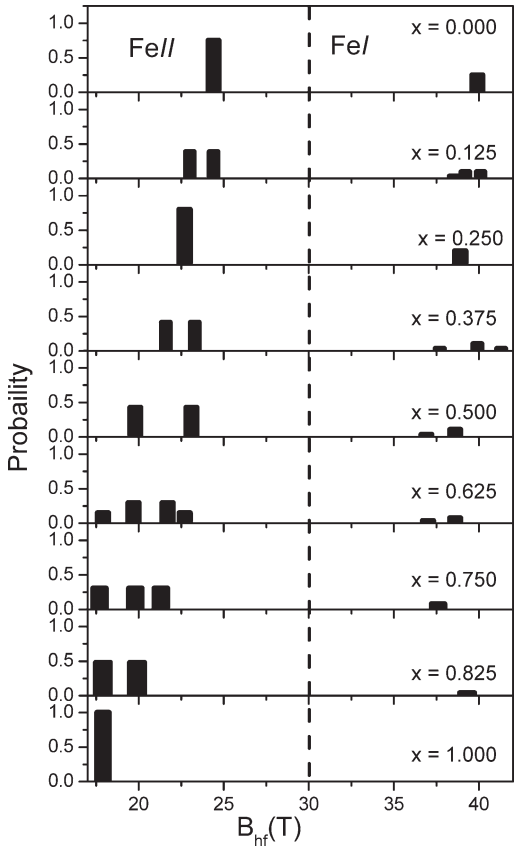

Figure 11. Theoretical probability distribution of magnetic hyperfine field labeled with the Ga content.

that it could differentiate the γ'-Fe_4N Mössbauer pattern from the $Ga_xFe_{4-x}N$ ones, as well as those of the intermediate concentrations.

5. CONCLUSIONS

By use of ab initio calculations it was possible to study the variations of the lattice parameter, magnetic, and hyperfine properties of the $Ga_xFe_{4-x}N$ compound with Ga content.

The nonlinear increase of the lattice parameter with x was ascribed to the different metallic radii of Ga and Fe atoms and a magneto-volumetric effect. Similar behavior of the lattice parameter with x has been reported experimentally.

The decrease of the M_{fu} was related to that Ga as a nonmagnetic element suppresses the Fe magnetism by dilution. Where, the difference between the up and down populations of the d-FeI orbitals does not change with Ga content, since the magnetic moment of the FeI atoms does not change with x. The magnetic moment of the FeII atoms decreases linearly with x, specifically with the amount of nnn Ga, because the chemical bonding (partly covalent) between them suppresses the Fe magnetism and a transfer of electronic states up to down keeping constant the total charge of the d-FeII orbitals.

To probe deeper in to the analysis of the structural and magnetic stability of $GaFe_3N$, fixed spin moment calculations were used to determine ferrimagnetic ground state, with a lattice parameter similar to the experimental value. Moreover, a strong dependence between the lattice parameter and the M_{fu} was observed, where the lattice parameter of the nonmagnetic state is smaller than the ferrimagnetic state ones.

The hyperfine parameters, B_{hf}, δ, and ε, of the FeI atoms do not change with x, whereas for the FeII atoms the B_{hf} linearly decreases with the amount of Ga nnn because of a transfer of up to down electronic states close to the nucleus. Finally, the linear increase of δ and ε with the amount of nnn Ga was observed, showing a loss of electronic charge in the orbitals close to the nucleus as well as a greater spherical asymmetry of these orbitals. The disclosed hyperfine distributions indicate that quite different patterns should be expected depending on the Ga content.

AUTHOR INFORMATION

Corresponding Author

*Phone/fax: +54 221 4236690. E-mail: eitelpyb@ing.unlp.edu.ar.

ACKNOWLEDGMENT

Research Grants PIP 0230 from Consejo Nacional de Investigaciones Científicas y Técnicas (CONICET, Argentina) and PICT 38047 and PICT 2042 from the Agencia Nacional de Promoción Científica y Tecnológica are gratefully recognized.

REFERENCES

(1) Suzuki, S.; Sakumoto, H.; Minegishi, J.; Omote, Y. *IEEE Trans. Magn.* **1981**, *17*, 3017–3019.
(2) Tasaki, A.; Tagawa, K.; Kita, E.; Harada, S.; Kusunose, T. *IEEE Trans. Magn.* **1981**, *17*, 3026–3028.
(3) Jacobs, H.; Rechenbach, D.; Zachwieja, U. *J. Alloys Compd.* **1995**, *227*, 10–17.
(4) Kuhnen, C. A.; de Figueiredo, R. S.; Drago, V. *J. Magn. Magn. Mater.* **1992**, *111*, 95–104.
(5) Chen, S. K.; Jin, S.; Tiefel, T. H.; Hsieh, Y. F.; Gyorgy, E. M.; Johnson, D. W., Jr. *J. Appl. Phys.* **1991**, *70*, 6247–6249.
(6) Andriamandroso, D.; Matar, S.; Demazeau, G.; Fournès, L. *IEEE Trans. Magn.* **1993**, *29*, 2–6.
(7) Houben, A.; Müller, P.; von Appen, J.; Lueken, H.; Niewa, R.; Dronskowski, R. *Angew. Chem., Int. Ed.* **2005**, *44*, 7212–7215.
(8) von Appen, J.; Dronskowski, R. *Angew. Chem., Int. Ed.* **2005**, *44*, 1205–1210.
(9) Krause, J. C.; Paduani, C. *Phys. B* **2005**, *367*, 282–286.
(10) Paduani, C. *J. Magn. Magn. Mater.* **2004**, *278*, 231–236.
(11) Frazer, B. C. *Phys. Rev.* **1958**, *112*, 751–754.
(12) Sakuma, A. *J. Magn. Magn. Mater.* **1991**, *102*, 127–134.
(13) Coehoorn, R.; Daalderop, G. H. O.; Jansen, H. J. F. *Phys. Rev. B* **1993**, *48*, 3830–3834.
(14) Ishida, S.; Kitawatase, K. *J. Magn. Magn. Mater.* **1992**, *104*, 1933–1934.
(15) Matar, S.; Mohn, P.; Demazeau, G.; Siberchicot, B. *J. Phys.* **1988**, *49*, 1761–1768.
(16) Peltzer y Blancá, E. L.; Desimoni, J.; Christensen, N. E. *Hyperfine Interact.* **2005**, *161*, 197–202.
(17) Peltzer y Blancá, E. L.; Desimoni, J.; Christensen, N. E.; Emmerich, H.; Cottenier, S. *Phys. Status Solidi B* **2009**, *246*, 909–928.
(18) Gil Rebaza, A. V.; Desimoni, J.; Peltzer y Blancá, E. L. *Physica B* **2009**, *404*, 2872–2875.
(19) Adler, J. F.; Williams, Q. *J. Geophys. Res.* **2005**, *110*, B01203–B01213.
(20) Kong, Y.; Diao, X. G.; Yang, J. B.; Li, F. S. *J. Magn. Magn. Mater.* **1997**, *172*, L15–L18.
(21) Yang, C. L.; Abd-Elmeguid, M. M.; Micklitz, H.; Michels, G.; Otto, J. W.; Kong, Y.; Xue, D. S.; Li, F. S. *J. Magn. Magn. Mater.* **1995**, *151*, L19–L23.
(22) Lord, J. S.; Armitage, J. G. M.; Riedi, P. C.; Matar, S. F.; Demazeau, G. *J. Phys.: Condens. Matter* **1994**, *6*, 1779–1790.
(23) Jack, K. H. *Proc. Roy. Soc. A* **1948**, *195*, 34–40.

(24) Shirane, G.; Takei, W. J.; Ruby, S. L. *Phys. Rev.* **1962**, *126*, 49–52.
(25) Music, D.; Schneider, J. M. *Appl. Phys. Lett.* **2006**, *88*, 031914–031916.
(26) Xue, D.; Li, F.; Yang, J.; Kong, Y.; Gao, M. *J. Magn. Magn. Matter* **1997**, *172*, 165–172.
(27) Mohn, P.; Schwarz, K.; Matar, S.; Demazeau, G. *Phys. Rev. B* **1992**, *45*, 4000–4007.
(28) Kong, Y.; Li, F. *Phys. Rev. B* **1998**, *57*, 970–977.
(29) Panda, R. N.; Gajbhiye, N. S. *J. Appl. Phys.* **1999**, *86*, 3295–3302.
(30) Diao, X. G.; Takeuchi, A. Y.; Garcia, F.; Scorzelli, R. B.; Rechenberg, H. R. *J. Appl. Phys.* **1999**, *85*, 4485–4487.
(31) El Khiraoui, S.; Sajieddine, M.; Vergat, M.; Sahlaoui, M.; Bauer, Ph.; Mabrouki, M. *J. Alloys Compd.* **2007**, *440*, 43–45.
(32) Wu, Y. Q.; Yan, M. F. *Phys. B* **2010**, *405*, 2700–2705.
(33) Wiener, G. W.; Berger, J. A. *J. Met.* **1955**, *7*, 360.
(34) Cordier-Robert, C.; Foct, J. *Eur. J. Solid State Inorg. Chem.* **1992**, *29*, 39.
(35) Kuhnen, C. A.; dos Santos, A. V. *J. Alloys Compd.* **2000**, *297*, 68–72.
(36) Stadelmaier, H. H.; Frazer, A. C. *Trans. Metall. Soc. AIME* **1960**, *218*, 571.
(37) Matar, S.; Mohn, P.; Kübler, J. *J. Magn. Magn. Mater.* **1992**, *104*, 1927–1928.
(38) dos Santos, A. V.; Kuhnen, C. A. *J. Alloys Compd.* **2001**, *321*, 60–66.
(39) Wu, Z.; Meng, J. *Appl. Phys. Lett.* **2007**, *90*, 241901–24193.
(40) Ma, X. G.; Jiang, J. J.; Liang, P.; Wang, J.; Ma, Q.; Zhang, Q. K. *J. Alloys Compd.* **2009**, *480*, 475–480.
(41) Matar, S.; Fournes, L.; ChéRubin-Jeanette, S.; Demazeau, G. *Eur. J. Solid State Inorg. Chem.* **1993**, *30*, 871–881.
(42) Houben, A.; Sepelak, V.; Becker, K. D.; Dronskowski, R. *Chem. Mater.* **2009**, *21*, 784–788.
(43) Zhao, E.; Xiang, H.; Meng, J.; Wu, Z. *Chem. Phys. Lett.* **2007**, *449*, 96–100.
(44) dos Santos, A. V.; Kuhnen, C. A. *J. Solid State Chem.* **2009**, *182*, 3183–3187.
(45) Cordier-Robert, C. PhD Thesis, USTL, Lille, France 1989.
(46) Matar, S. F.; Demazeau, G.; Hagenmuller, P.; Armitage, J. G. M.; Riedi, P. C. *Eur. J. Solid State Inorg. Chem.* **1989**, *26*, 517.
(47) Siberchicot, B.; Matar, S. F.; Fournes, L.; Demazeau, G.; Hagenmuller, P. *J. Solid State Chem.* **1990**, *84*, 10–15.
(48) Pauling, L. *J. Am. Chem. Soc.* **1947**, *69*, 542–553.
(49) Stadelmaier, H. H.; Fraker, A. C. *Z. Metallkd.* **1962**, *53*, 48–51.
(50) Houben, A.; Burghaus, J.; Dronskowski, R. *Chem. Mater.* **2009**, *21*, 4332–4338.
(51) Kurian, S.; Bhattacharyya, S.; Desimoni, J.; Peltzer y Blancá, E. L.; Gil Rebaza, A. V.; Gajbhiye, N. S. *J. Phys. Chem. C* **2010**, *114*, 17542–17549.
(52) Burghaus, J.; Wessel, M.; Houben, A.; Dronskowski, R. *Inorg. Chem.* **2010**, *49*, 10148–10155.
(53) Hohenberg, P.; Kohn, W. *Phys. Rev.* **1964**, *136*, B864–B871.
(54) Kohn, W.; Sham, L. J. *Phys. Rev.* **1965**, *140*, A1133–A1138.
(55) Singh, D. *Planewaves Pseudopotentials and the LAPW Method*; Kluwer Academic Publishers: London, 1994.
(56) Martin, R. M. *Electronic Structure Basic Theory and Practical Methods*; Cambridge University Press: New York, 2004.
(57) Blaha, P.; Schwarz, K.; Luitz, J.; Madsen, G. K. H.; Kvasnicka, D. *WIEN2K*; Technical University of Vienna: Vienna, Austria, 2001.
(58) Perdew, J. P.; Burke, K.; Ernzerhof, M. *Phys. Rev. Lett.* **1996**, *77*, 3865–3868.
(59) Murnaghan, F. D. *Finite deformation of an elastic solid*; John Wiley and Sons, Inc.: New York, 1951.
(60) Birch, F. *Phys. Rev.* **1947**, *71*, 809–824.
(61) Jacob, K. T.; Raj, S.; Rannesh, L. *Int. J. Mat. Res.* **2007**, *09*, 776–779.
(62) Dubiel, S. M. *J. Alloys Compd.* **2009**, *488*, 18–22.
(63) Blügel, S.; Akai, H.; Zeller, R.; Dederichs, P. H. *Phys. Rev. B* **1987**, *35*, 3271–3283.
(64) Vértes, A.; Korecz, L. Burger, K. *Mössbauer Spectroscopy*; Elsevier/North-Holland Inc.: Amsterdam, 1979.
(65) Eriksson, O.; Svane, A. *J. Phys.: Condens. Matter.* **1989**, *1*, 1589–1599.
(66) Dufeck, P.; Blaha, P.; Schwarz, K. *Phys. Rev. Lett.* **1995**, *75*, 3545–3548.
(67) Aldred, A. T. *J. Appl. Phys.* **1966**, *37*, 1344–1346.
(68) Blachowski, A.; Ruebenbauer, K.; Zukrowski, J.; Przewoznik, J. *J. Alloys Compd.* **2008**, *455*, 47–51.
(69) Newkirk, L. R.; Tsuei, C. C. *Phys. Rev. B* **1971**, *4*, 4046–4053.